Mechanisms of network collapse in GeO_2 glass: High-pressure neutron diffraction with isotope substitution as arbitrator of competing models

Kamil Wezka[1], Philip S Salmon[1], Anita Zeidler[1], Dean A J Whittaker[1], James W E Drewitt[1], Stefan Klotz[2], Henry E Fischer[3] and Dario Marrocchelli[4]

[1] Department of Physics, University of Bath, Bath BA2 7AY, UK
[2] IMPMC, Université Pierre et Marie Curie, 75252 Paris, France
[3] Institut Laue Langevin, 6 rue Jules Horowitz, BP 156, 38042 Grenoble, France
[4] School of Chemistry, Trinity College Dublin, College Green, Dublin 2, Ireland

E-mail: p.s.salmon@bath.ac.uk

Abstract. The structure of the network forming glass GeO_2 is investigated by making the first application of the method of *in situ* neutron diffraction with isotope substitution at pressures increasing from ambient to 8 GPa. Of the various models, the experimental results are in quantitative agreement only with molecular dynamics simulations made using interaction potentials that include dipole-polarisation effects. When the reduced density $\rho/\rho_0 \gtrsim 1.16$, where ρ_0 is the value at ambient pressure, network collapse proceeds via an interplay between the predominance of distorted square pyramidal GeO_5 units versus octahedral GeO_6 units as they replace tetrahedral GeO_4 units. This replacement necessitates the formation of threefold coordinated oxygen atoms and leads to an increase with density in the number of small rings, where a preference is shown for 6-fold rings when $\rho/\rho_0 = 1$ and 4-fold rings when $\rho/\rho_0 = 1.64$.

PACS numbers: 61.43.Fs, 61.05.fm, 62.50.-p, 64.70.kj

1. Introduction

The structural changes in glasses and liquids induced by high-pressure and/or high-temperature conditions can alter substantially their dynamical and transport properties [1, 2, 3, 4]. A notable example is provided by so-called polyamorphic transitions where the variation of a state parameter such as pressure or temperature leads to an abrupt transformation between two phases having the same composition but different densities [1, 2, 3, 4, 5, 6, 7]. Unravelling the mechanisms by which these transformations occur is, however, a formidable task owing to the nature of structural disorder [4, 8] and the experimental difficulties associated with the investigation of materials under extreme conditions [9, 10, 11, 12, 14, 13]. Notwithstanding these challenges, structural transformations offer an excellent opportunity for testing the efficacy of models used to predict the physical properties of glasses and liquids.

In this article, we approach these issues by making the first use of the method of *in situ* neutron diffraction with isotope substitution (NDIS) to measure the high-pressure structure of a glass, chosen to be GeO_2 on account of its scientific interest and the availability of suitable germanium isotopes [15]. Like silica and BeF_2, GeO_2 is a prototypical "strong" network glass-forming system [1, 16] for which significant structural changes occur as the material transforms to a high density polyamorph, often regarded as a more "fragile" counterpart to the ambient pressure material [1, 9, 14, 17, 18, 19, 20, 21, 22, 23, 24]. The transformations in GeO_2 occur at lower pressures by comparison with silica, making them more amenable to study by *in situ* high-pressure experiments [18, 21, 25], which are necessary to avoid relaxation of the glass on recovery to ambient conditions [9, 14, 26]. The real-space results obtained from conventional neutron diffraction [14, 27] and extended x-ray absorption fine structure (EXAFS) spectroscopy [17, 22, 24] experiments on GeO_2 glass are limited to a description of the Ge-O nearest-neighbours, although x-ray diffraction experiments also provide some information on the Ge-Ge correlations [9, 14, 23]. It is therefore necessary to have more detailed and unambiguous structural information on e.g. the O-O correlations in this oxide glass in order to test the veracity of the various models that have been proposed for the mechanisms of pressure-driven network collapse [9, 28, 29, 30, 31, 32, 33, 34].

The NDIS method has played a key role in revealing the structure of multi-component glasses and liquids [8, 35, 36]. It is, however, challenging to apply this method to high-pressure investigations because the sample sizes are necessarily small ($1-3\%$ of the amount of material in a typical ambient pressure NDIS experiment [37, 38]), the use of high-pressure apparatus leads to detrimental background scattering, and neutron diffraction is a flux-limited probe by comparison with x-ray diffraction. Recently, much effort has been devoted to the instrumentation and methodology required to make accurate measurements of the neutron diffraction patterns for glasses and liquids at pressures within the $\sim 1-20$ GPa regime [14, 27]. The progress made has facilitated the present *in situ* NDIS experiment which is designed to *resolve* the nearest-neighbour Ge-

Ge and O-O correlations and hence provide previously unknown information on e.g. the intra-polyhedral O-Ge-O and inter-polyhedral Ge-O-Ge bond-angle distributions. We find that, of the various models available, the NDIS results are in agreement only with molecular dynamics simulations based on the method described by Marrocchelli *et al* [39, 34]. Additional quantitative information is thereby gained on the nature of the structural transformations that occur.

The manuscript is organized as follows. The essential theory for the neutron diffraction experiments is given in section 2. The experimental and molecular dynamics methods are then described in sections 3 and 4, respectively. The results are presented in section 5 and are discussed in section 6 where attention is focussed on the nature of five-fold coordinated Ge atoms and the pressure dependence of the ring statistics. Conclusions are drawn in section 7.

2. Theory

In a neutron diffraction experiment the total structure factor

$$F(Q) = \sum_{\alpha=1}^{n} \sum_{\beta=1}^{n} c_\alpha c_\beta b_\alpha b_\beta \left[S_{\alpha\beta}(Q) - 1 \right] \tag{1}$$

is measured where α and β denote the chemical species, n is the number of different chemical species, c_α and b_α represent the atomic fraction and bound coherent scattering length of chemical species α, $S_{\alpha\beta}(Q)$ is a partial structure factor and Q is the magnitude of the scattering vector [36]. The corresponding real-space information is represented by the total pair-distribution function $G(r)$ which is obtained from $F(Q)$ by Fourier transformation.

Let diffraction experiments be made on three samples of GeO_2 glass that are identical in every respect, except for their Ge isotopic enrichments. If the samples are $^{\rm nat}GeO_2$, $^{70}GeO_2$ and $^{73}GeO_2$ then the total structure factors $^{\rm nat}F(Q)$, $^{70}F(Q)$ and $^{73}F(Q)$ are measured, respectively, where nat denotes the natural isotopic abundance of germanium. The complexity of correlations associated with a single total structure factor can be simplified by forming the first-difference function $^{X-Y}\Delta F_{\rm Ge}(Q)$ to eliminate the O-O partial structure factor where

$$\begin{aligned} {}^{X-Y}\Delta F_{\rm Ge}(Q) &\equiv {}^{X}F(Q) - {}^{Y}F(Q) \\ &= 2c_{\rm Ge}c_{\rm O}b_{\rm O}\left(b_{X\,{\rm Ge}} - b_{Y\,{\rm Ge}}\right)\left[S_{\rm GeO}(Q) - 1\right] \\ &+ c_{\rm Ge}^2\left(b_{X\,{\rm Ge}}^2 - b_{Y\,{\rm Ge}}^2\right)\left[S_{\rm GeGe}(Q) - 1\right] \end{aligned} \tag{2}$$

and X, Y denote nat, 70 or 73 with $X \neq Y$. Alternatively, the Ge-Ge partial structure factor can be eliminated by forming the weighted first-difference function

$$\begin{aligned} {}^{X-Y}\Delta F_{\rm O}(Q) &\equiv \left[b_{Y\,{\rm Ge}}^2\,{}^{X}F(Q) - b_{X\,{\rm Ge}}^2\,{}^{Y}F(Q)\right] / \left(b_{Y\,{\rm Ge}}^2 - b_{X\,{\rm Ge}}^2\right) \\ &= 2c_{\rm Ge}c_{\rm O}b_{\rm O}b_{Y\,{\rm Ge}}b_{X\,{\rm Ge}}\left(b_{Y\,{\rm Ge}} + b_{X\,{\rm Ge}}\right)^{-1}\left[S_{\rm GeO}(Q) - 1\right] \\ &+ c_{\rm O}^2 b_{\rm O}^2\left[S_{\rm OO}(Q) - 1\right]. \end{aligned} \tag{3}$$

Table 1. The weighting coefficients for the Ge-O, Ge-Ge and O-O partial structure factors for several of the measured difference functions defined by equations (2) and (3). The numerical values take into account the isotopic enrichments of the samples used for the experiments (see section 3).

Function	Ge-O (barn)	Ge-Ge (barn)	O-O (barn)
$^{70-73}\Delta F_{\mathrm{Ge}}(Q)$	0.124(3)	0.081(2)	–
$^{\mathrm{nat}-73}\Delta F_{\mathrm{Ge}}(Q)$	0.078(1)	0.0450(6)	–
$^{70-73}\Delta F_{\mathrm{O}}(Q)$	0.0875(5)	–	0.1497(2)
$^{\mathrm{nat}-73}\Delta F_{\mathrm{O}}(Q)$	0.0815(4)	–	0.1497(2)

The weighting coefficients for the partial structure factors for several of the measured difference functions are listed in table 1.

The real-space functions associated with $^{X-Y}\Delta F_{\mathrm{Ge}}(Q)$ and $^{X-Y}\Delta F_{\mathrm{O}}(Q)$ are obtained from the Fourier transform relation

$$^{X-Y}\Delta G_{\mathrm{Ge/O}}(r) = \frac{1}{2\pi^2\rho r}\int_0^\infty {}^{X-Y}\Delta F_{\mathrm{Ge/O}}(Q)M(Q)\sin(Qr)QdQ \qquad (4)$$

where ρ is the atomic number density of the glass and $M(Q)$ is a modification function defined by $M(Q) = 1$ for $Q \leq Q_{\mathrm{max}}$, $M(Q) = 0$ for $Q > Q_{\mathrm{max}}$ which is introduced because a diffractometer can measure only over a finite Q range up to a maximum value Q_{max}. To facilitate a comparison between the molecular dynamics and experimental results, the reciprocal-space functions constructed from the simulations were Fourier transformed according to equation (4) with Q_{max} set at the experimental value. We note that if Q_{max} is sufficiently large such that the difference functions no longer show structure at high Q, then $^{X-Y}\Delta G_{\mathrm{Ge}}(r)$ and $^{X-Y}\Delta G_{\mathrm{O}}(r)$ follow from equations (2) and (3), respectively, by replacing each $S_{\alpha\beta}(Q)$ by its corresponding partial pair-distribution function $g_{\alpha\beta}(r)$.

In principle, the full set of partial structure factors can be extracted from the high-pressure data sets, as in the case of GeO_2 glass under ambient conditions [37, 38]. In practice, however, the experimental uncertainties resulting e.g. from the counting statistics were found to be too large. Notwithstanding, the measurement of three $F(Q)$ functions and their associated difference functions enables consistency checks to be made on the results to test their accuracy. In the following, the $^{X-Y}\Delta F_{\mathrm{Ge}}(Q)$ and $^{X-Y}\Delta F_{\mathrm{O}}(Q)$ functions obtained from the pairs of total structure factors $^{70}F(Q)$ and $^{73}F(Q)$ or $^{\mathrm{nat}}F(Q)$ and $^{73}F(Q)$ are presented since these correspond to the largest contrast between the scattering lengths of the germanium isotopes.

3. Experimental

Samples of glassy $^{\mathrm{nat}}GeO_2$ (Alfa-Aesar, 99.9999%), $^{70}GeO_2$ (97.71% ^{70}Ge, 2.23% ^{72}Ge, 0.02% ^{73}Ge, 0.03% ^{74}Ge, 0.01% ^{76}Ge) and $^{73}GeO_2$ (0.04% ^{70}Ge, 2.84% ^{72}Ge, 96.07%

^{73}Ge, 1.03% ^{74}Ge, 0.02% ^{76}Ge) were prepared by quenching melts from 1400 °C [27]. The scattering lengths, taking into account the isotopic enrichments, are $b_{^{\rm nat}{\rm Ge}} = 8.185(20)$, $b_{^{70}{\rm Ge}} = 9.96(10)$, $b_{^{73}{\rm Ge}} = 5.15(4)$ and $b_{\rm O} = 5.803(4)$ fm [15]. The experiments were made at ambient temperature ($T \sim 300$ K) and used the diffractometer D4c at the Institut Laue-Langevin [40].

The high-pressure diffraction experiment employed a VX5/180 type Paris-Edinburgh press (piston area of 66.5 cm^2) with cubic BN anvils having a single-toroid profile. Since the sample position changes with the piston displacement upon increasing the applied load, the press was mounted on a platform that could be translated vertically (z-axis drive) so that the sample could be centred in the incident beam at each pressure point with the aid of an optical camera. The background scattering was minimised by optimising the setup given in [14]. The samples for the high-pressure runs were prepared by using an identical procedure in which pellets of the correct geometry for the anvils were made by pre-compacting finely powdered glass. They were held in gaskets made from a $Ti_{0.676}Zr_{0.324}$ alloy which has a zero coherent neutron scattering length. The sample masses, as measured at the end of the high-pressure runs, showed that the number of scattering centres for the $^{70}GeO_2$ and $^{73}GeO_2$ samples matched the number for the $^{\rm nat}GeO_2$ sample to within 3.2%. The incident neutron wavelength of $\lambda = 0.6947(1)$ Å and zero scattering angle for the detectors were measured using Ni powder contained within an encapsulated $Ti_{0.676}Zr_{0.324}$ gasket [41] mounted in the Paris-Edinburgh press with no applied load. Higher order ($\lambda/2$) scattering was suppressed by placing an Ir filter after the Cu(200) monochromator, upstream of the sample position.

For a given sample, the diffraction pattern for an empty Ti-Zr gasket was first measured with a small applied load. The sample was then mounted in this gasket and diffraction patterns were measured for different pressures, where the load on the anvils was always increased during the course of a high-pressure run. Diffraction patterns were also measured for (a) several empty Ti-Zr gaskets that had been recovered from different high pressures in order to estimate the gasket scattering under load, and (b) the empty anvils with different anvil separations in order to help in estimating the background scattering. To assist in the data normalisation at different pressures, where the anvils have different separations, additional diffraction patterns were measured at ambient pressure for large and small vanadium pellets contained in unsquashed and recovered (i.e. previously squashed) Ti-Zr gaskets, respectively. The data analysis followed the procedure described elsewhere [14].

The sample pressure P was deduced from the load applied to the anvils of the press by using a calibration curve that has been extensively checked [14, 27]. At several of the pressure points, in order to assess the sensitivity of the results to the applied load, the latter was varied about its desired value by up to 3.4 tonnes (corresponding to a change in sample pressure of ~ 0.3 GPa) and diffraction patterns were measured. For a given pressure point, this variation of load did not give rise to a notable change in the diffraction patterns within the counting statistics.

The ambient-pressure diffraction experiment used a different experimental setup

in which powdered glass samples were held in a vanadium container of inner diameter 4.8 mm and 0.1 mm wall thickness. The incident neutron wavelength was 0.6950(1) Å. Diffraction patterns were taken for each sample in its container, the empty container, the empty instrument, and a cylindrical vanadium rod of diameter 6.072(6) mm for normalisation purposes. A diffraction pattern was also measured for a bar of neutron absorbing $^{10}B_4C$ of dimensions comparable to the sample to account for the effect of the sample's attenuation on the background signal at small scattering angles. As for the high-pressure experiment, each complete diffraction pattern was built up from the intensities measured for different positions of D4c's group of nine microstrip detectors. These intensities were saved at regular intervals to check the sample and diffractometer stabilities. The data were analysed by using a standard procedure [42].

The supporting pillars of the Paris-Edinburgh press restrict the maximum accessible scattering angle as compared to the vanadium container experiment which did not employ high-pressure apparatus. The maximum cutoff value $Q_{\max}$ was therefore 15.3 Å^{-1} for the high-pressure experiment as compared to 16.9 Å^{-1} for the ambient-pressure experiment.

The final results at ambient pressure and at pressures of 4.0(5), 5.9(5), 6.8(5) and 8.0(5) GPa correspond to reduced sample number densities ρ/ρ_0 of 1, 1.156, 1.304 1.343 and 1.378, respectively, where $\rho_0 = 0.0629$ Å^{-3} is the ambient-pressure value [37, 38, 43].

4. Molecular Dynamics Simulations

The molecular dynamics simulations were made using the so-called DIPole-Polarisable Ion Model (DIPPIM) where the interaction potentials include dipole-polarisation effects. The potentials were parameterised by using *ab initio* simulations as opposed to experimental results and are therefore largely unbiased in their predictions of the glass structure [39]. The DIPPIM is the only model currently available that gives, for a single set of parameters, a good account of both the structural and vibrational properties of glassy GeO_2 at ambient pressure along with the dynamical properties of liquid GeO_2 at elevated temperatures [39]. The simulations of the glass were made at $T = 300$ K using a system of $N = 432$ atoms in the NVT ensemble where V denotes the volume of the system. The equations of motion were integrated using a time step of 1 fs, and the polarisation energy at each time step was minimised using a conjugate gradient method. An in-house code called PIMAIM was used for the calculations.

To obtain the glass at ambient pressure, GeO_2 was first liquified at high temperature (5000−10000 K), and a 1 ns long simulation was made at 4000 K. The system was then cooled down to room temperature at a rate of ~ 3.7 K/ps. A high-pressure state was subsequently obtained by using a cold-compression procedure [44] in which the cell lengths and particle positions were rescaled to the new density, a 1 ns long simulation was made to equilibrate the system, and data were collected during a further 1 ns run. A limited timescale is associated with the glass preparation procedure in the molecular dynamics simulations, in common with all standard simulation techniques, such that

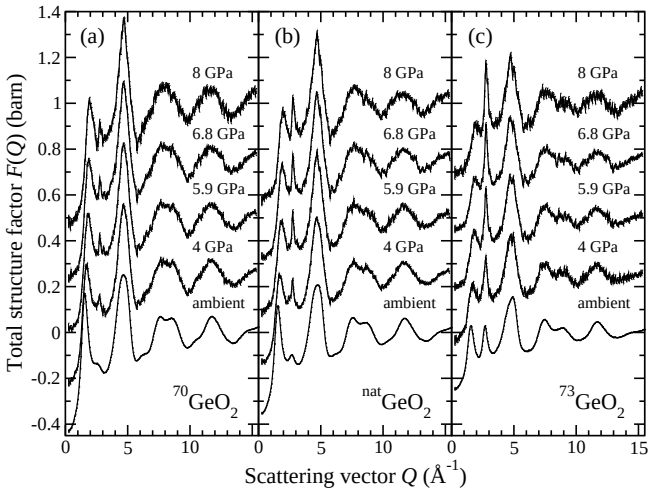

Figure 1. The pressure dependence of the measured total structure factors (a) $^{70}F(Q)$, (b) $^{\rm nat}F(Q)$ and (c) $^{73}F(Q)$ for GeO_2 glass. The vertical bars give the statistical errors on the measured data points. The high-pressure data sets have been shifted vertically for clarity of presentation.

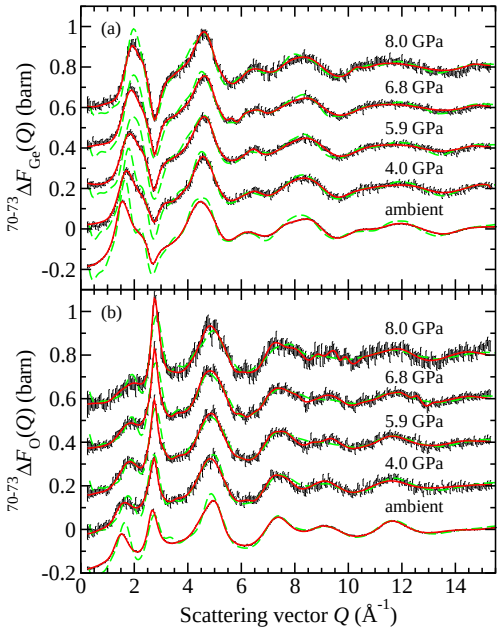

Figure 2. The pressure dependence of (a) $^{70-73}\Delta F_{\rm Ge}(Q)$ and (b) $^{70-73}\Delta F_{\rm O}(Q)$. The vertical bars give the statistical errors on the measured data points, the solid (red) curves give the Fourier transforms of the corresponding real-space functions shown in figure 4, and the broken (green) curves give the molecular dynamics results. The high-pressure data sets have been shifted vertically for clarity of presentation.

the equation of state for GeO_2 glass was not reproduced [34]. The simulations were therefore made with the glass density set at the value used to analyse the diffraction results. Where necessary, a density-to-pressure conversion was made using the data of Hong *et al* [43].

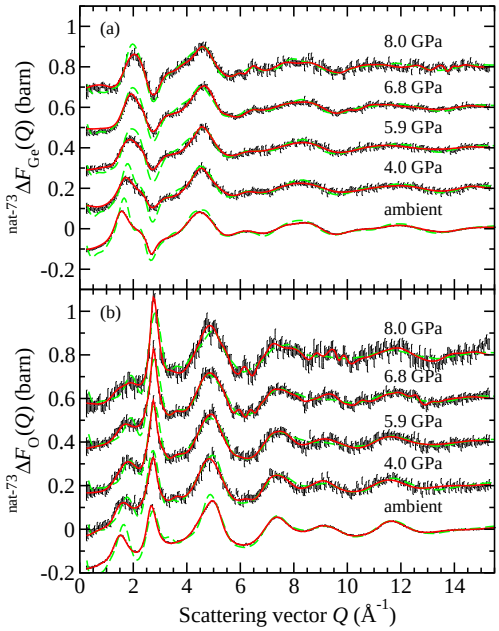

Figure 3. The pressure dependence of (a) $^{\mathrm{nat}-73}\Delta F_{\mathrm{Ge}}(Q)$ and (b) $^{\mathrm{nat}-73}\Delta F_{\mathrm{O}}(Q)$. The vertical bars give the statistical errors on the measured data points, the solid (red) curves give the Fourier transforms of the corresponding real-space functions shown in figure 5, and the broken (green) curves give the molecular dynamics results. The high-pressure data sets have been shifted vertically for clarity of presentation.

5. Results

The measured total structure factors show systematic changes with increasing pressure (figure 1). For example, each function has a first sharp diffraction peak at $\simeq$1.55 Å^{-1} under ambient conditions which moves to higher Q values and decreases in magnitude with increasing density, indicating a significant alteration to the intermediate range order [45]. In comparison, the principal peak at $\simeq$2.64 Å^{-1} under ambient conditions, which is associated with extended range ordering [37, 38], sharpens with increasing pressure. These changes are consistent with a competition between the intermediate and extended-range ordering which is won by the latter with increasing density as the glass transforms to a more "fragile" material [37, 46].

As shown by figures 2 and 3, the difference functions $^{70-73}\Delta F_{\mathrm{Ge}}(Q)$ and $^{\mathrm{nat}-73}\Delta F_{\mathrm{Ge}}(Q)$ show very similar features, in accordance with the relative weighting factors of the partial structure factors in equation (2). Likewise, the difference functions $^{70-73}\Delta F_{\mathrm{O}}(Q)$ and $^{\mathrm{nat}-73}\Delta F_{\mathrm{O}}(Q)$ show very similar features, in accordance with the relative weighting factors of the partial structure factors in equation (3). This demonstrates that, despite the difficulties in making *in situ* high pressure NDIS experiments, it is possible to measure reliable diffraction patterns.

The real-space functions $^{X-73}\Delta G_{\mathrm{Ge}}(r)$ and $^{X-73}\Delta G_{\mathrm{O}}(r)$ are shown in figures 4 and 5. As for the total pair-distribution functions $G(r)$, the first peak is attributable to Ge-O correlations and, for each pressure point, the various functions all yield the same Ge-O

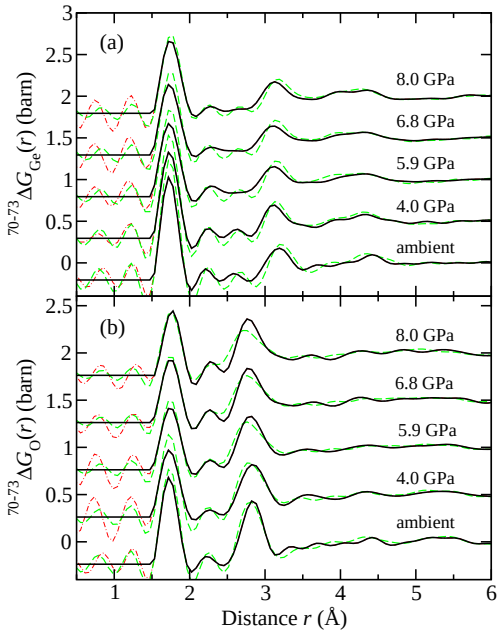

Figure 4. The pressure dependence of (a) $^{70-73}\Delta G_{\mathrm{Ge}}(r)$ and (b) $^{70-73}\Delta G_{\mathrm{O}}(r)$ (solid (black) curves), as obtained by spline fitting and Fourier transforming the measured reciprocal-space functions shown in figure 2, where the chained (red) curves show the unphysical small r oscillations. The broken (green) curves give the molecular dynamics results as obtained by Fourier transforming the simulated functions shown in figure 2 after applying the same maximum cutoff Q_{max} as for the neutron diffraction data (see equation (4)). The high-pressure data sets have been shifted vertically for clarity of presentation.

bond length r_{GeO} and coordination number $\bar{n}_{\mathrm{GeO}}$ for oxygen around germanium, within the experimental uncertainty. These results are compared in figure 6 to those obtained from previous neutron diffraction work [14, 27]. Importantly, the NDIS method also allows the nearest-neighbour Ge-Ge and O-O correlations to be *resolved*, as manifested by the second peaks in $^{X-73}\Delta G_{\mathrm{Ge}}(r)$ and $^{X-73}\Delta G_{\mathrm{O}}(r)$, respectively. The corresponding distances are plotted in figure 6 along with the O-O coordination number $\bar{n}_{\mathrm{OO}}$, obtained by assuming minimal overlap with the Ge-O correlations as observed under ambient conditions [38]. The mean O-Ge-O and Ge-O-Ge bond angles, deduced from the measured nearest-neighbour distances [46], are compared in figure 7 with those measured for the α-quartz polymorph of GeO_2 [47, 48]. To facilitate this comparison, the data are plotted as a function of the reduced density ρ/ρ_0.

In figures 2–7 the experimental data are compared to the new molecular dynamics results obtained by using the DIPPIM interaction potentials, and in every case there is excellent overall agreement. By contrast, other models for the pressure-induced structural changes in GeO_2, as obtained by using the Oeffner-Elliott potentials [49] in classical molecular dynamics simulations [28, 29, 30, 31, 32] or first principles molecular dynamics simulations [33], do not reproduce basic features such as the pressure dependence of the measured Ge-O bond lengths and coordination numbers (figure 8).

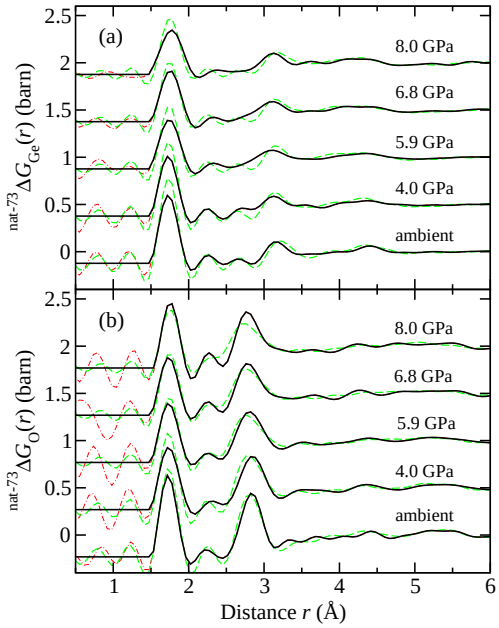

Figure 5. The pressure dependence of (a) $^{\mathrm{nat}-73}\Delta G_{\mathrm{Ge}}(r)$ and (b) $^{\mathrm{nat}-73}\Delta G_{\mathrm{O}}(r)$ (solid (black) curves), as obtained by spline fitting and Fourier transforming the measured reciprocal-space functions shown in figure 3, where the chained (red) curves show the unphysical small r oscillations. The broken (green) curves give the molecular dynamics results as obtained by Fourier transforming the simulated functions shown in figure 3 after applying the same maximum cutoff Q_{max} as for the neutron diffraction data (see equation (4)). The high-pressure data sets have been shifted vertically for clarity of presentation.

The following picture thus emerges for the structural evolution of compressed GeO_2 glass. When $\rho/\rho_0 < 1.16$ (or $P < 4.5$ GPa) there is little change in r_{GeO} or $\bar{n}_{\mathrm{GeO}}$ (figure 6). Compaction proceeds via a reorganisation of distorted corner-sharing tetrahedral GeO_4 units in which there is a reduction of the mean Ge-O-Ge bond angle, supporting an interpretation of Raman scattering results [18, 25], and an increase in $\bar{n}_{\mathrm{OO}}$. The rate of decrease of this bond angle with ρ/ρ_0 is similar to the α-quartz polymorph (figure 7(b)). On further densification, r_{GeO} and $\bar{n}_{\mathrm{GeO}}$ both increase and a second branch appears in both the O-Ge-O and Ge-O-Ge molecular dynamics bond-angle distributions. Initially, these changes correspond to a replacement of GeO_4 tetrahedra by GeO_5 units (figure 7(a)), and to maintain the glass stoichiometry threefold coordinated oxygen atoms must form (figure 7(b)). Signatures associated with the appearance of GeO_5 units are an increase and decrease in the rate of change with pressure of the O-Ge-O and Ge-O-Ge bond angles, respectively (figure 7), and an increase in the rate of change with pressure of the measured density [43, 27]. Subsequently, when $\rho/\rho_0 \gtrsim 1.4$, the tetrahedra are also replaced by octahedral GeO_6 units, the fraction of GeO_5 units reaching a maximum when $\rho/\rho_0 \simeq 1.57$. In comparison, $\rho/\rho_0 = 1.45$ for the ambient temperature transformation of GeO_2 at $P > 6$ GPa from the α-quartz to the monoclinic polymorph built from chains of edge-sharing GeO_6 octahedra [50].

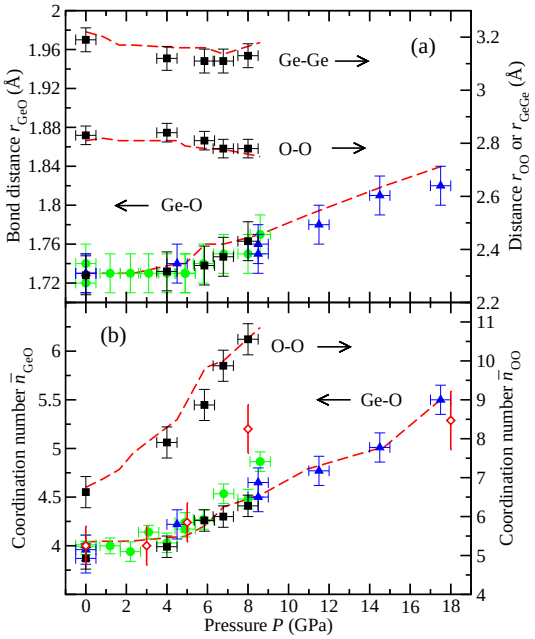

Figure 6. The pressure dependence of the nearest-neighbour (a) Ge-O, O-O and Ge-Ge distances and (b) the Ge-O and O-O coordination numbers. The results from the present neutron diffraction (■) and molecular dynamics [broken (red) curves] work are compared, where possible, to those obtained from the neutron diffraction studies of [14] [(green) •] and [27] [(blue) ▲]. The distances were taken from the peak positions in the real-space functions, except for the molecular dynamics Ge-O distance which was found using $\langle r_{\rm GeO}\rangle = \int {\rm d}r\, r g_{\rm GeO}(r) / \int {\rm d}r\, g_{\rm GeO}(r)$. The molecular dynamics $\bar{n}_{\rm OO}$ values were found by integrating $g_{\rm OO}(r)$ up to $r_{\rm max}$ as found from the second peak in the measured ${}^{70-73}\Delta G_{\rm O}(r)$ and ${}^{\rm nat-73}\Delta G_{\rm O}(r)$ functions (figures 4 and 5). In (b) the Ge-O coordination numbers from IXS experiments [54] are also shown [(red) ◇].

We note that, when the GeO_5 units appear at a reduced density $\rho/\rho_0 \gtrsim 1.16$, the first peak in the simulated partial pair-distribution function $g_{\rm GeO}(r)$ develops a high r tail (figure 9). This is not, however, seen as an obvious feature in the ${}^{X-73}\Delta G_{\rm Ge}(r)$ and ${}^{X-73}\Delta G_{\rm O}(r)$ functions plotted in figures 4 and 5 because the molecular dynamics data have been treated in the same way as the experimental results in order to respect the finite $Q_{\rm max}$ value (see equation (4)).

6. Discussion

The GeO_5 units found from the molecular dynamics simulations range from trigonal bipyramids, as seen in crystalline germanates [51, 52], to square pyramids where interconversion can be achieved via a minimal distortion of the intra-polyhedral O-Ge-O bond angles [53]. As indicated by figure 7(a), the O-Ge-O bond-angle distributions calculated for the GeO_5 units at the various pressures do not, however, show a peak or obvious shoulder at $\simeq$120° as anticipated for a significant fraction of trigonal bipyramids. Inspection of the GeO_5 conformations shows that most have a distorted square-pyramidal geometry described by $\tau \sim 40\%$ at all pressures, where τ is a parameter

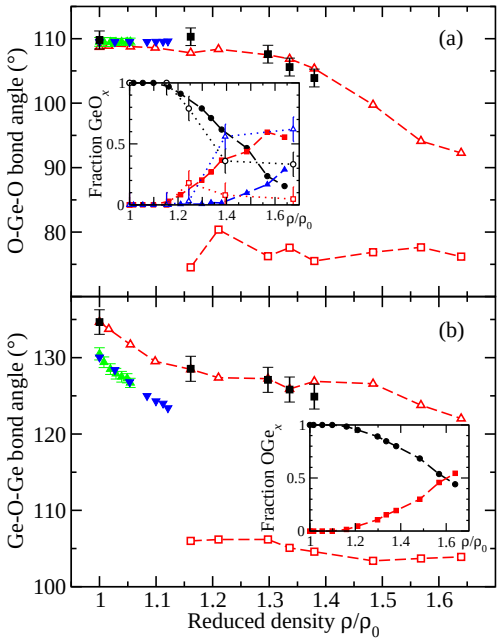

Figure 7. The reduced density ρ/ρ_0 dependence of (a) the O-Ge-O and (b) the Ge-O-Ge bond angles as measured in the present diffraction work on glassy GeO_2 (■) and in the diffraction work of [47] [(green) ▲] and [48] [(blue) ▼] on the α-quartz polymorph of crystalline GeO_2. Also shown are the molecular dynamics results for the glass where two branches appear, corresponding to a shoulder or peak in the bond-angle distributions. One branch originates at ambient density from tetrahedral GeO_4 motifs [(red) △)] and the other appears at higher densities [(red) □] as these motifs are replaced by GeO_5 and GeO_6 units. The insets show the molecular dynamics results for the density dependence of (a) the fraction of GeO_x species, where $x = 4$ (•), 5 [(red) ■] or 6 [(blue) ▲], and (b) the fraction of OGe_x species, where $x = 2$ (•) or 3 [(red) ■]. In (a), the inset also shows the fraction of GeO_x species from IXS experiments [54] where $x = 4$ (○), 5 [(red) □] or 6 [(blue) △].

that ranges from 0% for regular square pyramids to 100% for regular trigonal bipyramids [53]. Thus, with increasing density, there is initially a progression from tetrahedral to predominantly square pyramidal units, where the vacancy at the base of the latter anticipates the eventual formation of octahedral (i.e. square bipyramidal) units. The density dependence of GeO_x units ($x = 4$, 5 or 6) found from the present work contrasts with recent inelastic x-ray scattering (IXS) experiments (figure 7(a)), perhaps due to use of data from crystalline standards containing trigonal bipyramidal GeO_5 units to analyse the IXS spectra measured for the glass [54]. The corresponding Ge-O coordination numbers are compared to the neutron diffraction results in figure 6(b).

To gain further insight into the nature of the pressure-driven network collapse, the configurations generated from the molecular dynamics simulations were analysed by making a shortest-path search for rings containing either n Ge atoms or n O atoms by employing the Rigorous Investigation of Networks Generated using Simulation (RINGS) code [55]. These searches were initiated either from Ge atoms or from O atoms and were restricted to looking for successive neighbours of unlike chemical species. In the RINGS

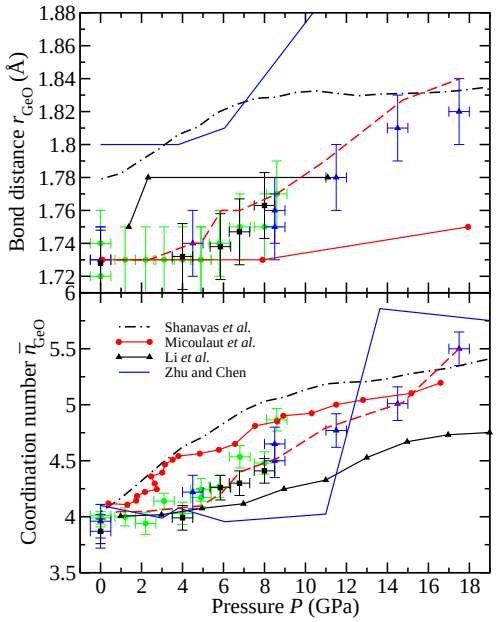

Figure 8. The pressure dependence of the Ge-O bond distance and coordination number in GeO_2 glass. The data points from neutron diffraction are shown by the various symbols with error bars as defined in the figure 6 caption. The curves give the results obtained from various molecular dynamics simulations where those using the DIPPIM interaction potentials of Marrocchelli *et al* [39] are given by the broken light (red) curves and are in agreement with the experimental data. In contrast, the molecular dynamics simulations of Micoulaut *et al* [28, 29] (solid (red) curves with circles), Shanavas *et al* [30] (chained dark (black) curves) and Li *et al* [32] (solid (black) curves with triangles) using the Oeffner-Elliott interaction potentials [49], and the first principles molecular dynamics simulations of Zhu and Chen [33] (solid dark (blue) curves), are not consistent with the measured data sets.

analysis, $R_c(n)$ is the number of n-fold rings normalised to the total number of atoms in the model. $P_N(n)$ is the number of Ge (or O) atoms used in finding at least one ring containing n atoms, normalised to the total number of Ge (or O) atoms. $P_{\rm max}(n)$ and $P_{\rm min}(n)$ are the probabilities that, for a given Ge (or O) atom in an n-fold ring, the ring is either the longest or shortest closed path that can be found by using this same atom to initiate a search, respectively.

The dependence on reduced density of the connectivity profiles obtained when using Ge atoms to initiate shortest path searches is shown in figure 10. The maximum in $R_c(n)$ at $n = 8$ for $\rho/\rho_0 = 1$ compares to a maximum at $n = 6{-}7$ from other molecular dynamics simulations [31, 56]. The formation of edge-sharing GeO_5 polyhedra at $\rho/\rho_0 \simeq 1.16$ manifests itself by the appearance of $n = 2$ rings and, as their number increases with ρ/ρ_0, there is a shift in the distribution of rings to smaller sizes. When $\rho/\rho_0 > 1.16$ the increase in number of $n = 3$ rings, attributed to the D_2 band at $\simeq 520$ cm^{-1} in Raman spectra [56, 57], is consistent with the measured density dependence of this feature [18, 25, 21]. The peak in $P_N(n)$ shows that the ring size for the majority of Ge atoms changes from $n = 6$ at ambient density to $n = 4$ at $\rho/\rho_0 = 1.64$.

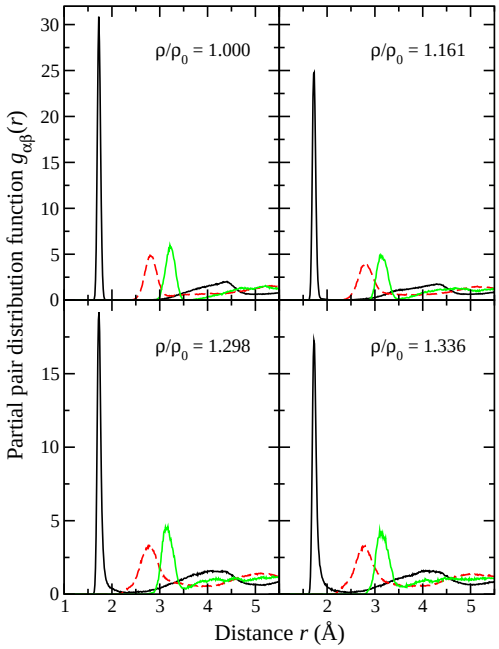

Figure 9. The Ge-O (dark solid (black) curves), O-O (broken (red) curves) and Ge-Ge (light solid (green) curves) partial pair-distribution functions from molecular dynamics simulations using the DIPPIM interaction potentials at several reduced densities.

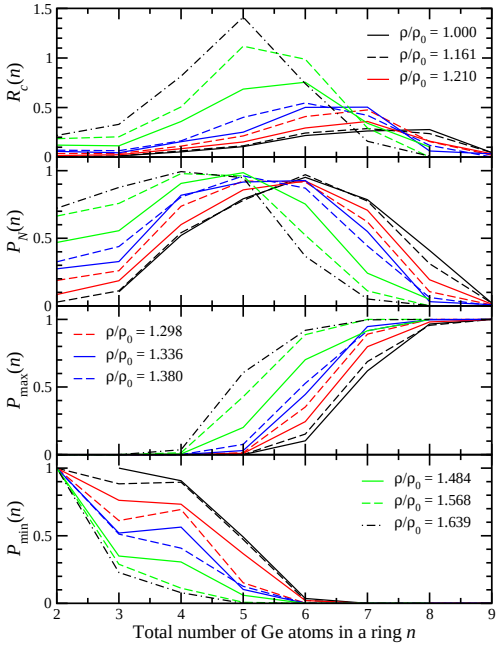

Figure 10. The connectivity profiles $R_c(n)$, $P_N(n)$, $P_{\max}(n)$ and $P_{\min}(n)$ as calculated for the molecular dynamics configurations for GeO_2 glass at different reduced densities ρ/ρ_0 by using the RINGS code [55]. The searches were initiated from Ge atoms and were restricted to looking for successive neighbours of unlike chemical species.

The dependence on reduced density of the connectivity profiles obtained when using oxygen atoms to initiate shortest path searches is shown in figure 11. When GeO_5 units

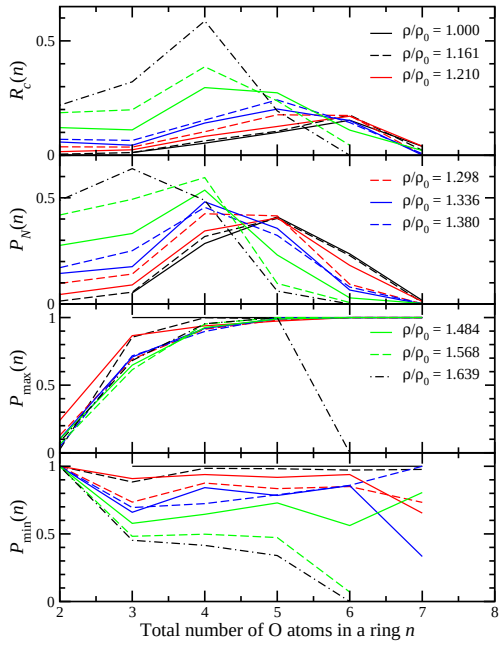

Figure 11. The connectivity profiles $R_c(n)$, $P_N(n)$, $P_{\max}(n)$ and $P_{\min}(n)$ as calculated for the molecular dynamics configurations for GeO_2 glass at different reduced densities ρ/ρ_0 by using the RINGS code [55]. The searches were initiated from O atoms and were restricted to looking for successive neighbours of unlike chemical species.

appear at $\rho/\rho_0 \simeq 1.16$, threefold coordinated oxygen atoms also appear and there is a change in the values of $P_{\min}(n)$ and $P_{\max}(n)$ from unity i.e. the increased connectivity of the oxygen atoms leads to the possibility that they will be involved in more than one type of ring.

7. Conclusions

In summary, we have shown that the NDIS method can be used to help disentangle the structural complexity of disordered materials *in situ* under high pressure conditions, thus providing detailed experimental information to test the efficacy of different structural models. In the case of GeO_2 glass, quantitative agreement is found between the NDIS measurements and molecular dynamics simulations made by using transferable interatomic potentials that include dipole-polarisation effects, an agreement that spans self-consistently a good number of structural parameters. At elevated densities, the interplay between GeO_4, GeO_5 and GeO_6 polyhedra shows that two-state models [3, 4, 17, 19] will not provide a reliable account of the pressure-induced structural transformations.

Acknowledgments

We thank Adrian Barnes (Bristol), Mathieu Salanne (Paris), Sébastien Le Roux (Strasbourg) and Julien Haines (Montpellier) for useful discussions, Gérald Lelong

(Paris) for providing the data sets from [54], Alfredo Pasquarello (Lausanne) for providing his code to calculate τ, Paul Reddish (Bath) for machining the Ti-Zr gaskets, and Alain Bertoni, Jean-Luc Laborier and Claude Payre (ILL) for help with the diffraction experiments. The experimental work benefitted from the award of long term proposal LTP-6-1 at the Institut Laue-Langevin. It also benefitted from EPSRC support to the Bath group via grants to PSS and AZ (EP/G008795/1 and EP/J009741/1) and via PhD studentships to KW, DAJW and JWED. DM wishes to thank the Government of Ireland for an EMPOWER Postdoctoral Fellowship and the Trinity Centre for High Performance Computing for computing time.

References

[1] Angell C A 1995 *Science* **267** 1924
[2] Brazhkin V V and Lyapin A G 2003 *J. Phys.: Condens. Matter* **15** 6059
[3] Wilding M C, Wilson M and McMillan P F 2006 *Chem. Soc. Rev.* **35** 964
[4] Greaves G N and Sen S 2007 *Adv. Phys.* **56** 1
[5] Greaves G N, Wilding M C, Fearn S, Langstaff D, Kargl F, Cox S, Vu Van Q, Majérus O, Benmore C J, Weber R, Martin C M, and Hennet L 2008 *Science* **322** 566
[6] Barnes A C, Skinner L B, Salmon P S, Bytchkov A, Pozdnyakova I, Farmer T O and Fischer H E 2009 *Phys. Rev. Lett.* **103** 225702; 2011 *Phys. Rev. Lett.* **106** 119602
[7] Daisenberger D, Deschamps T, Champagnon B, Mezouar M, Cabrera R Q, Wilson M and McMillan P F 2011 *J. Phys. Chem B* **115** 14246
[8] Cusack N E 1987 *The Physics of Structurally Disordered Matter* (Bristol, Hilger)
[9] Guthrie M, Tulk C A, Benmore C J, Xu J, Yarger J L, Klug D D, Tse J S, Mao H-k, and Hemley R J 2004 *Phys. Rev. Lett.* **93** 115502
[10] Wilding M, Guthrie M, Bull C L, Tucker M G and McMillan P F 2008 *J. Phys.: Condens. Matter* **20** 244122
[11] Soignard E, Benmore C J and Yarger J L 2010 *Rev. Sci. Instrum.* **81** 035110
[12] Price D L 2010 *High-Temperature Levitated Materials* (Cambridge, CUP).
[13] Klotz S 2012 *Techniques in High Pressure Neutron Scattering* (Boca Raton, CRC Press).
[14] Drewitt J W E, Salmon P S, Barnes A C, Klotz S, Fischer H E and Crichton W A 2010 *Phys. Rev. B* **81** 014202
[15] Sears V F 1992 Neutron News **3** (Number 3) 26
[16] Wilson M and Salmon P S 2009 *Phys. Rev. Lett.* **103** 157801
[17] Itié J P, Polian A, Calas G, Petiau J, Fontaine A and Tolentino H 1989 *Phys. Rev. Lett.* **63** 398
[18] Durben D J and Wolf G H 1991 *Phys. Rev. B.* **43** 2355
[19] Smith K H, Shero E, Chizmeshya A and Wolf G H 1995 *J. Chem. Phys.* **102** 6851
[20] Tsiok O B, Brazhkin V V, Lyapin A G and Khvostantsev L G 1998 *Phys. Rev. Lett.* **80** 999
[21] Micoulaut M, Cormier L and Henderson G S 2006 *J. Phys.: Condens. Matter* **18** R753
[22] Vaccari M, Aquilanti G, Pascarelli S and Mathon O 2009 *J. Phys.: Condens. Matter* **21** 145403
[23] Mei Q, Sinogeikin S, Shen G, Amin S, Benmore C J and Ding K 2010 *Phys. Rev. B* **81** 174113
[24] Baldini M, Aquilanti G, Mao H-k, Yang W, Shen G, Pascarelli S and Mao W L 2010 *Phys. Rev. B* **81** 024201
[25] Polsky C H, Smith K H and Wolf G H 1999 *J. Non-Cryst. Solids* **248** 159
[26] Sampath S, Benmore C J, Lantzky K M, Neuefeind J, Leinenweber K, Price D L and Yarger J L 2003 *Phys. Rev. Lett.* **90** 115502
[27] Salmon P S, Drewitt J W E, Whittaker D A J, Zeidler A, Wezka K, Bull C L, Tucker M G, Wilding M C, Guthrie M and Marrocchelli D 2012 *J. Phys.: Condens. Matter* **24** 415102
[28] Micoulaut M 2004 *J. Phys.: Condens. Matter* **16** L131

[29] Micoulaut M, Guissani Y and Guillot B 2006 *Phys. Rev. E* **73** 031504
[30] Shanavas K V, Garg N and Sharma S M 2006 *Phys. Rev. B* **73** 094120
[31] Micoulaut M, Yuan X and Hobbs L W 2007 *J. Non-Cryst. Solids* **353** 1961
[32] Li T, Huang S and Zhu J 2009 *Chem. Phys. Lett.* **471** 253
[33] Zhu X F and Chen L F 2009 *Physica B* **404** 4178
[34] Marrocchelli D, Salanne M and Madden P A 2010 *J. Phys.: Condens. Matter* **22** 152102
[35] Enderby J E, North D M and Egelstaff P A 1966 *Phil. Mag.* **14** 961
[36] Fischer H E, Barnes A C and Salmon P S 2006 *Rep. Prog. Phys.* **69** 233
[37] Salmon P S, Barnes A C, Martin R A and Cuello G J 2006 *Phys. Rev. Lett.* **96** 235502
[38] Salmon P S, Barnes A C, Martin R A and Cuello G J 2007 *J. Phys.: Condens. Matter* **19** 415110
[39] Marrocchelli D, Salanne M, Madden P A, Simon C and Turq P 2009 *Mol. Phys.* **107** 443
[40] Fischer H E, Cuello G J, Palleau P, Feltin D, Barnes A C, Badyal Y S and Simonson J M 2002 *Appl. Phys. A* **74** S160
[41] Marshall W G and Francis D J 2002 *J. Appl. Cryst.* **35** 122
[42] Salmon P S, Xin S and Fischer H E 1998 *Phys. Rev. B* **58** 6115
[43] Hong X, Shen G, Prakapenka V B, Newville M, Rivers M L and Sutton S R 2007 *Phys. Rev. B* **75** 104201
[44] Liang Y, Miranda C R and Scandolo S 2008 *High Pressure Res.* **28** 35
[45] Salmon P S 1994 *Proc. R. Soc. Lond. A* **445** 351
[46] Salmon P S 2007 *J. Phys.: Condens. Matter* **19** 455208
[47] Jorgensen J D 1978 *J. Appl. Phys.* **49** 5473
[48] Glinnemann J, King Jr H E, Schulz H, Hahn Th, La Placa S J and Dacol F 1992 *Z. Kristallogr.* **198** 177
[49] Oeffner R D and Elliott S R 1998 *Phys. Rev. B* **58** 14791
[50] Haines J, Léger J M and Chateau C 2000 *Phys. Rev. B* **61** 8701
[51] Fáy E, Völlenkle H and Wittmann A 1973 *Z. Kristallogr.* **138** 439
[52] Harbrecht B, Kushauer J and Weber H-J 1990 *Eur. J. Solid State Inorg. Chem.* **27** 831
[53] Pasquarello A, Petri I, Salmon P S, Parisel O, Car R, Tóth E, Powell D H, Fischer H E, Helm L and Merbach A E 2001 *Science* **291** 856
[54] Lelong G, Cormier L, Ferlat G, Giordano V, Henderson G S, Shukla A and Calas G 2012 *Phys. Rev. B* **85** 134202
[55] Le Roux S and Jund P 2010 *Comput. Mater. Sci.* **49** 70; 2011 *Comput. Mater. Sci.* **50** 1217
[56] Giacomazzi L, Umari P and Pasquarello A 2006 *Phys. Rev. B* **74** 155208
[57] Giacomazzi L, Umari P and Pasquarello A 2005 *Phys. Rev. Lett.* **95** 075505